# Injection locking of two laterally-coupled semiconductor laser arrays

Nianqiang Li, Hadi Susanto, Benjamin Cemlyn, Ian Henning, Michael Adams

Nianqiang Li, Hadi Susanto, Benjamin Cemlyn, Ian Henning, Michael Adams, "Injection locking of two laterally-coupled semiconductor laser arrays," Proc. SPIE 10682, Semiconductor Lasers and Laser Dynamics VIII, 106820Z (9 May 2018); doi: 10.1117/12.2306158

SPIE.

Event: SPIE Photonics Europe, 2018, Strasbourg, France

# Injection locking of two laterally-coupled semiconductor laser arrays

Nianqiang Li*[a], Hadi Susanto[b], Benjamin Cemlyn[a], Ian Henning[a], and Michael Adams[a]
[a]School of Computer Science and Electronic Engineering, University of Essex, Wivenhoe Park, Colchester CO4 3SQ, UK; [b]Department of Mathematical Sciences, University of Essex, Wivenhoe Park, Colchester CO4 3SQ, UK

## ABSTRACT

In this paper the injection locking properties of two laterally-coupled semiconductor lasers (LCSLs) are studied numerically. We consider external injection into either one (single external-injection scheme) or both (simultaneous external-injection scheme) of the LCSLs. We present stability maps for both schemes in the plane of the frequency detuning and the injection strength, where attention is centered on the influence of the waveguiding structures, the laser separation, the pump rate, and the frequency offset between the two coupled lasers. Our results contribute to a better understanding of LCSLs under external injection.

**Keywords:** laterally-coupled semiconductor laser arrays, injection locking, external injection, waveguiding structures

## 1. INTRODUCTION

Semiconductor laser arrays coupled evanescently have attracted considerable attention since they allow for stable high-power operation in a narrow beam[1,2] as well as yielding a rich variety of dynamics[3-12]. Among these, two laterally-coupled semiconductor lasers (LCSLs), as the simplest laser arrays, have already been extensively studied in terms of stability and dynamics[13-18]. It has been demonstrated both theoretically and experimentally that these devices are intrinsically unstable under certain conditions and can develop complicated dynamics including periodicity, quasiperiodicity and even chaos[13,18]. These complex dynamics may have potential applications to microwave generation[19] as well as chaos-based secure communications[20] and random bit generators[21]. However, dynamic instabilities are not desirable for all situations and sometimes stable steady-state operation is more desirable[1,2]. Thus optical injection locking has been widely used for stabilization in laser systems[22-25], which in addition results in modulation bandwidth enhancement[26]. This is also the case for LCSL arrays. Mercier and McCall studied the stability and dynamics of an injection-locked semiconductor laser array with two evanescently coupled lasers under simultaneous external injection[27]. Goldberg et al. reported their experiments on the injection locking of 10-element laser arrays to a single-mode master laser, where similar results were achieved when either the entire array or only one of the elements was illuminated by the master laser[28]. Despite the existence of these important studies of injection locking of LCSL arrays, a comprehensive understanding of the mechanisms, the injection-locking characteristics, and the effects of some key parameters on the locking region for the case of simultaneous or single external injection remain unclear.

In our previous work[29], we found that in four representative laser waveguide structures ranging from those with purely real guidance to a combination of index antiguiding and gain-guiding there exists a periodicity of behaviour with laser separation that was overlooked in the literature. We extended this study by introducing optical injection into one element of the two LCSLs and discovered an interesting trapezoidal locking region[30]. In both studies, analytic approximation, a path continuation technique and direct numerical integration of the rate equation based on coupled mode theory were used and good agreement was found between these methods. In the current contribution we carry out a detailed theoretical study on the injection locking of two LCSLs, where both lasers are either under simultaneous external injection or only one of them is subject to external injection. We compare four different waveguiding structures and show the influence of other key parameters viz. the laser separation, pump rate, and frequency offset between the two coupled lasers.

*Corresponding author. Email address: wan_103301@163.com

Semiconductor Lasers and Laser Dynamics VIII, edited by Krassimir Panajotov, Marc Sciamanna, Rainer Michalzik,
Proc. of SPIE Vol. 10682, 106820Z · © 2018 SPIE · CCC code: 0277-786X/18/$18 · doi: 10.1117/12.2306158

## 2. THEORETICAL MODEL

We are interested in two LCSLs where either one or both are subject to external injection, which is termed single and simultaneous external-injection scheme, respectively. To model them, we follow the configuration illustrated schematically in Fig. 1 of our prior work[29], and consider two identical laser waveguides, A and B, each of width $2a$, with an edge-to-edge separation of $2d$, mutually coupled through the evanescent tails of their fields. To be more precise, for the single external-injection scheme, an additional degree of freedom is introduced whereby laser A is subject to continuous-wave optical injection from a master laser, similar to our previous modeling[30]. In the case of the simultaneous external-injection scheme, both laser A and laser B are subject to continuous-wave optical injection from a master laser, corresponding to the scheme considered by Mercier and McCall[27]. In both schemes, the frequency of the master laser can be detuned relative to those of the two-element laser array.

The coupled-mode equations for our laser model can be written as

$$\frac{dE_A}{dt} = \Gamma \frac{c}{2n_g} a_{diff} \left(N_A - N_{Ath}\right)\left(1 - i\alpha_H\right) E_A + i\left(\omega - \Omega_A\right) E_A + i\eta E_B + k_{inj} E_{inj} e^{-i\Delta\omega t}, \quad (1)$$

$$\frac{dE_B}{dt} = \Gamma \frac{c}{2n_g} a_{diff} \left(N_B - N_{Bth}\right)\left(1 - i\alpha_H\right) E_B + i\left(\omega - \Omega_B\right) E_B + i\eta E_A + k_{inj} E_{inj} e^{-i\Delta\omega t}, \quad (2)$$

$$\frac{dN_{A,B}}{dt} = P_{A,B} - \frac{N_{A,B}}{\tau_N} - \frac{c}{n}\left[g_{A,Bth} + a_{diff}\left(N_{A,B} - N_{A,Bth}\right)\right]\left|E_{A,B}\right|^2, \quad (3)$$

where the subscript A, B stands for laser A, B, $E_{A,B}$ are the electric fields, and $N_{A,B}$ are the carrier concentrations (with the subscript '*th*' indicating the threshold values). The third terms on the right side of the first two equations stand for the lateral-coupling effect between the two lasers of the array, with $\eta$ the complex coupling coefficient. In Eq. (14) of[29] this rate is expressed in terms of amplitude and phase parameters $C_\eta$, $C_\theta$ (found from numerical integration) and $W_r$, $W_i$ which are the real and imaginary parts of the transverse propagation constant in the regions outside the cores of waveguides A and B. The last terms represent the external injection from a master laser, where $\Delta\omega = \omega_{inj} - \omega$, with $\omega_{inj}$ as the injected angular frequency and $\omega$ as the free-running angular frequency of the total electric field of the system in the absence of injection, $E_{inj}$ as the injected field, and $k_{inj}$ as a coupling rate for the injected signal. For the single external-injection scheme, the last term in Eq. (2) does not exist for the laser B. Other parameters are the optical confinement factor $\Gamma$, the speed of light $c$, the group index $n_g$, the differential gain, the linewidth enhancement factor $\alpha_H$, the frequencies $\Omega_{A,B}$, the pump rate $P_{A,B}$, the carrier lifetime $\tau_N$, the refractive index $n$ and the threshold gain $g_{th}$.

In the current study, we present our results in the form of stability maps distinguishing the steady-state operation and the oscillatory behavior in the plane of the frequency detuning $\Delta f = \Delta\omega/2\pi$ and the injection strength $K$ defined as $K = k_{inj}\tau_N E_{inj} \big/ \left|E_{A,B}\right|$.

In our numerical simulations, a fourth-order Runge-Kutta algorithm has been used to solve Eqs. (1)-(3). The following set of parameter values is considered[29,30]: $\alpha_H = 2$, $a = 4\ \mu\text{m}$, $a_{diff} = 1\times10^{-15}\ \text{cm}^2$, $N_o = 1\times10^{18}\ \text{cm}^{-3}$, $\tau_N = 1.0\ \text{ns}$, $\tau_p = 1.53\ \text{ps}$, and $n = 3.4$. These values are fixed throughout the current study as they are typical for LCSLs. We restrict attention to the case of equal pumping in each laser, so that $P \equiv P_A = P_B$, which is expressed in terms of the ratio to its threshold value $P/P_{th}$. For consistency we study the influence of waveguiding structures based on the cases analyzed in[29,30], summarized below in Table 1, where $\Delta n_r$ and $\Delta n_i$ are the real and imaginary parts of the index difference between the core and cladding regions of the waveguides and $C_Q = N_o\, a_{diff} / g_{th}$. The first is purely real index guiding, the second positive index guiding with gain-guiding, the third pure gain guiding (no built-in index guiding) and the last index antiguiding with gain-guiding . Although we assume the two lasers are nominally identical, we do allow for a static

difference in lasing frequency ($\Delta\Omega/2\pi = (\Omega_B - \Omega_A)/2\pi$) between them which might occur in practice either unintentionally as a result of small fabrication variations or by design. We refer to this as the 'offset frequency', or simply as the 'offset'.

**Table 1. Values of key parameters for modeling, using material parameter values given in[29,30].**

| $\Delta n_r$ | $g_{th}$ (cm$^{-1}$) | $\Delta n_i$ | $W_r$ | $W_i$ | $C_Q$ | $C_\eta$ (ns$^{-1}$) | $C_\theta$ (rad) |
|---|---|---|---|---|---|---|---|
| 0.00097 | 87.7 | 0 | 1.26 | 0 | 11.4 | 83.6 | 0 |
| 0.0005 | 90.6 | 0.000937 | 1.09 | 0.896 | 11.0 | 90.2 | 0.233 |
| 0 | 99.3 | 0.00103 | 0.795 | 1.22 | 10.1 | 91.9 | 0.294 |
| -0.0005 | 108 | 0.00112 | 0.604 | 1.61 | 9.26 | 96.3 | 0.183 |

# 3. RESULTS

In this section, numerical results for the injection-locking properties of two LCSLs subject to external injection are presented. We present the results in the form of stability maps plotted in the plane of the injection strength $K$ and the frequency detuning $\Delta f$ .

## 3.1 Single external-injection scheme

In our previous work[30], the locking conditions and bandwidth for the single external-injection scheme have been clarified. The important findings can be summarized as follows. First, both lasers can be injection-locked in the same region under suitable conditions. The upper and lower limits of the trapezoidal injection-locking region are two parallel saddle-node bifurcation curves, which confine an uninterrupted steady-state region especially for weak coupling. Second, as the laser separation increases, the locking region shrinks in size, which gives rise to a narrower locking bandwidth. Third, the offset tunes the locking domain, which means the locking region can be shifted vertically on the map of ( $K$ , $\Delta f$ ) by gradually varying this offset parameter. More importantly, these findings are not restricted by waveguiding structure but uncover a generic locking behavior. It is worthwhile to note that we only considered a fixed pump rate $P = 2P_{th}$ in[30]. It is important to be aware of the influence of the pump rate on the locking domain since it is an experimentally controllable parameter. As noted in[30] and above, similar locking behavior would be expected for the four waveguiding structures specified in Table 1. For illustrative purposes, our attention is focused mainly on the purely real index guiding, i.e., parameters specified in the first row of Table 1.

Figure 1 presents the stability maps in the ( $K$ , $\Delta f$ ) plane for three different but fixed pump rates, i.e., $P = 1.1P_{th}$ , $P = 2P_{th}$ , and $P = 5P_{th}$ , where the offset $\Delta\Omega/2\pi = -6$ GHz . As we shall further discuss the influence of the laser separation, two values of $d/a$ , i.e., 1.2 and 1.4, are considered. For illustrative purposes, the locked region is represented by blue, while the unstable regions are represented by yellow. For the pump rate $P = 2P_{th}$ (middle row) the locking region is symmetric with respect to the offset $\Delta\Omega/2\pi = -6$ GHz . For a lower pump rate $P = 1.1P_{th}$ (upper row), the locking domain becomes much narrower and does not show symmetry as mentioned above. This is because part of the locking range is interrupted by oscillations originating from Hopf bifurcations, which is similar to the case where $P = 2P_{th}$ but for smaller $d/a$ , as shown in Fig. 6 of[30]. In the case of much higher pump rates, e.g., $P = 5P_{th}$ (bottom row), one can observe an uninterrupted injection locking domain again. It is interesting to see that its size and location are exactly the same as $P = 2P_{th}$ . This means that the absolute locking region is independent of the pump rate if it exceeds a critical value. In fact, this has been mathematically predicted in Eq. (13) of[30] where the contribution from the pump rate is negligible and omitted. The good agreement between the numerical results and analytical approximation is also indicated in the case of $P = 5P_{th}$ . It should be noted that in all cases of Fig. 1, only the results for laser A are shown since those for laser B are the same; increasing $d/a$ results in the shrinkage of the locking domain. However, as $d/a$ is further increased to a very large value, the evanescent coupling between lasers A and B becomes extremely weak, which dramatically changes the locking of the two LCSLs.

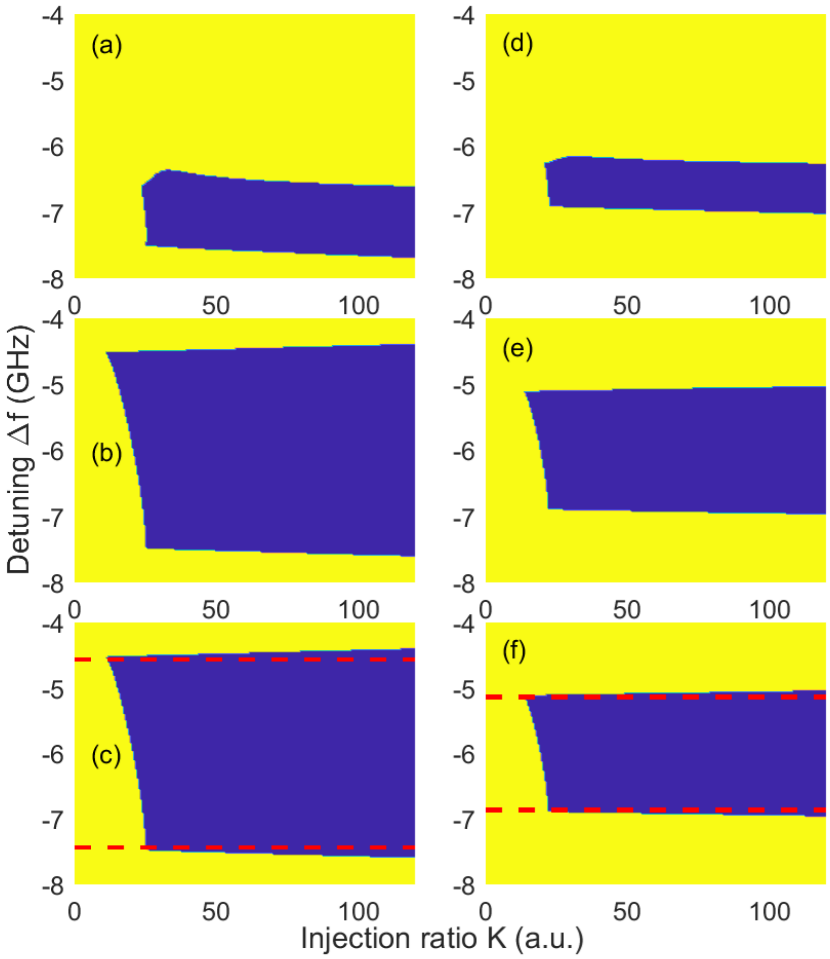


Figure 1. Stability diagram of two LCSLs under single external injection in the ( $K$ , $\Delta f$ ) plane, where $\Delta\Omega/2\pi = -6$ GHz . First row: $P = 1.1P_{th}$ , second row: $P = 2P_{th}$ , and third row: $P = 5P_{th}$ . Left column: $d/a = 1.2$ , and right column: $d/a = 1.4$ . The dashed lines in the third row are plotted based on Eq. (13) of[30]. In all cases, blue stands for stability, while yellow for instability; only the results for laser A are shown. Here, the purely real index guiding is considered.

In Fig. 2, we show an example for large values of $d/a$ , i.e., $d/a = 8$ , with $P = 2P_{th}$ and $\Delta\Omega/2\pi = -6$ GHz . For comparison, the results for both laser A and laser B are shown. From Fig. 2(a), we see that the locking region for laser A is greatly expanded and, resembles the shape for a solitary laser subject to external injection[22]. However, in Fig. 2(b), we observe that laser B operates in the steady state in the whole parameter space considered. We believe that this is expected since for such a large d/a, the coupling between the two LCSLs is negligible, so that the whole system is divided into a single optically injected laser (laser A) and a free-running laser (laser B). Similar to the case of $P = 5P_{th}$ shown in Fig. 1, the lower limit (red dashed; saddle-node bifurcation) of the locking boundaries is depicted in Fig. 2(a), which is well approximated by using Eq. (14) of[30].

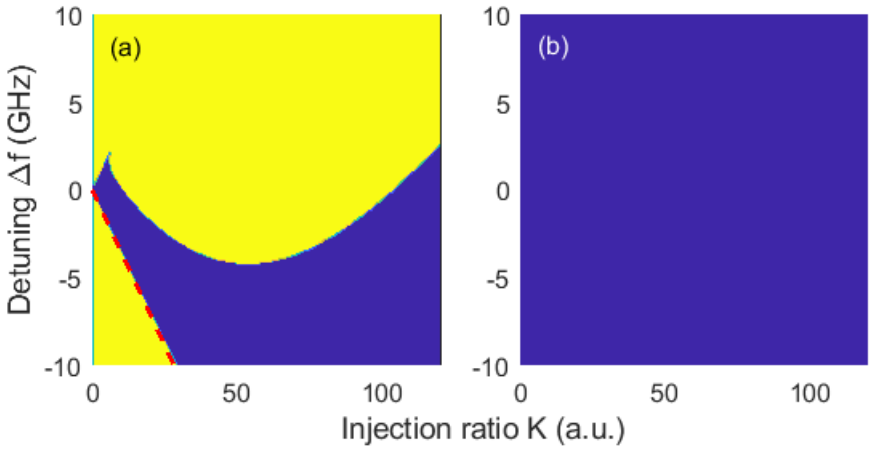


Figure 2. Stability diagram of two LCSLs under single external injection in the ( $K$ , $\Delta f$ ) plane, where $\Delta\Omega/2\pi = -6$ GHz , $P = 2P_{th}$ , and $d/a = 8$ . (a) laser A, and (b) laser B. The dashed line in (a) is plotted based on Eq. (14) of[30].Here, the purely real index guiding is considered.

### 3.2 Simultaneous external-injection scheme

We now concentrate on the case of simultaneous external injection. We start our investigation with the purely real index guiding for zero offset, i.e., both lasers in the array are exactly identical. As before, stability diagrams are used to distinguish the locked (blue) and unstable (yellow) regions and clarify the influence on them of some key parameters.

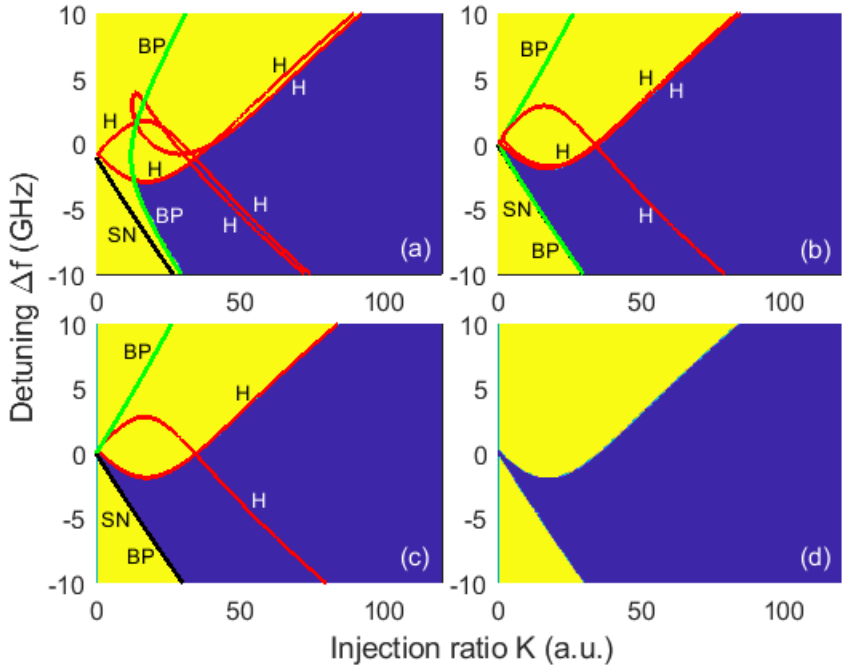


Figure 3. Stability diagram of two LCSLs under simultaneous external injection in the ( $K$ , $\Delta f$ ) plane, where $P = 1.1P_{th}$ and $\Delta\Omega/2\pi = 0$ GHz . (a) $d/a = 1$ , (b) $d/a = 2$ , (c) $d/a = 3$ , and (d) $d/a = 10$ . Red curve stands for Hopf (H), green for pitchfork (BP), and black for saddle-node (SN). Here, the purely real index guiding is considered and only the results for laser A are shown.

Figure 3 illustrates the results for $P = 1.1P_{th}$ and four different but fixed values of $d/a$. In all cases considered here, both lasers can be simultaneously locked in the same region highlighted in blue, and thus only the results for laser A are shown. At relatively small values of $d/a$, the left-most point of the stability map is located at negative values of $\Delta f$ and nonzero values of $K$; see Fig. 3(a) for $d/a = 1$, for example. For a relatively large value, the left-most point is moved to zero values of $K$ and $\Delta f$, as shown in Fig. 3(b) for $d/a = 2$. As $d/a$ is further increased and beyond a critical value, the stability diagrams remain unchanged, similar to the case of a single laser subject to external injection[22]. This is evident by comparing Figs. 3(c) and 3(d), where $d/a = 3$ and $d/a = 10$, respectively. To gain more insight into the nature of the locking boundary, we also show the key bifurcation curves obtained by using the standard continuation package AUTO[31,32]. As shown in Fig. 3(a), the upper locking boundary is formed by parts of two Hopf bifurcation curves and the lower boundary by part of a pitchfork bifurcation curve. The appearance of the pitchfork bifurcation originates from the symmetry property, since no offset is introduced between the two LCSLs. For comparison, the saddle-node curve is also shown in this figure, although it does not confine the locking region. As $d/a$ is increased, the two Hopf bifurcations delimiting the upper limit become almost overlapped, and this is also the case for the saddle-node and pitchfork bifurcations for the lower limit [see Fig. 3(b)]. In Fig. 3(c), only one Hopf curve governs the upper limit, while for the lower limit the saddle-node curve and the pitchfork curve become indistinguishable by eye. The results in Fig. 3(d) are the same as Fig. 3(c), so bifurcations are not repeated here.

Next we consider the influence of the offset. Fig. 4 shows the results for $\Delta\Omega/2\pi = -2$ GHz and $-6$ GHz, while other parameters are the same as those in Fig. 3(b). When compared to Fig. 3(b), it is interesting to find that the stable region is only bounded by one Hopf curve and one saddle-node curve in the presence of an offset between the two LCSLs. The disappearance of the pitchfork bifurcation is expected due to the offset, which destroys the symmetry in the laser array. Moreover, it is of interest to find that the upper limit is shifted vertically in frequency by an amount almost equal to the predetermined offset, which results in the left-most point of the locking region being moved to a more negative frequency and a larger injection strength as the absolute value of the offset becomes greater.

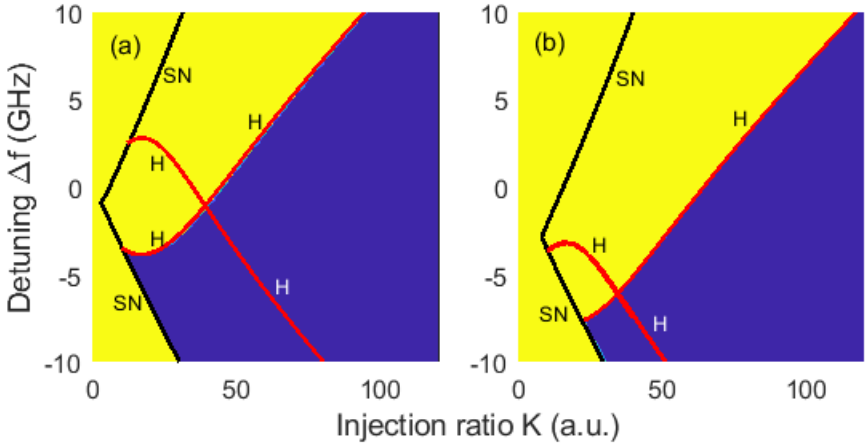


Figure 4. Stability diagram of two LCSLs under simultaneous external injection in the ($K$, $\Delta f$) plane, where $P = 1.1P_{th}$ and $d/a = 2$. (a) $\Delta\Omega/2\pi = -2$ GHz, and (b) $\Delta\Omega/2\pi = -6$ GHz. Here, the purely real index guiding is considered, and the results for laser A are shown.

Similar to the single injection case, here we also consider the influence of the pump rate. The results for $P = 2P_{th}$ are shown in Fig. 5, where two values of the offset are considered. It is clearly seen that at higher injection levels the upper boundary (i.e. the Hopf curve) of the locked region moves to more negative detuning frequencies with increasing pump rate. In addition a shift in frequency almost equal to the offset is also observed by comparing Figs. 5(a) and (b). Note that in Fig. 5(b), a wider range of the vertical axis is used. A comparison between Figs. 4 and 5 shows that the locking region shrinks in size as the pump rate is increased in the parameter space considered in both figures.

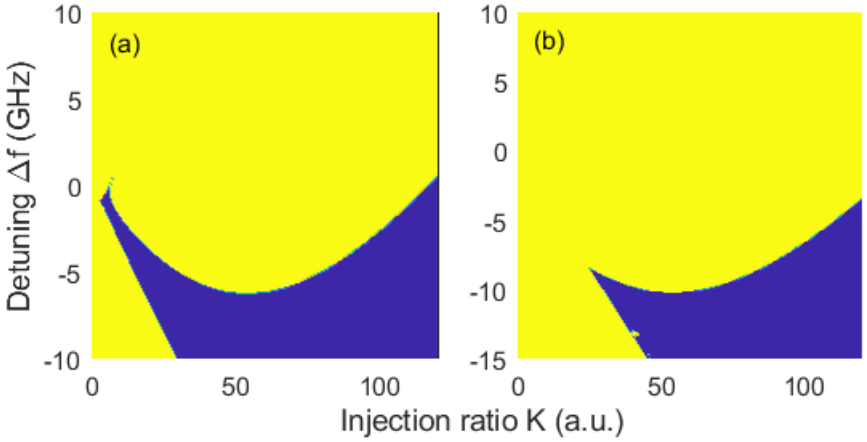


Figure 5. Stability diagram of two LCSLs under simultaneous external injection in the ( $K$ , $\Delta f$ ) plane, where $P = 2P_{th}$ and $d/a = 2$ . (a) $\Delta\Omega/2\pi = -2$ GHz , and (b) $\Delta\Omega/2\pi = -6$ GHz . Here, the purely real index guiding is considered, and only the results for laser A are shown.

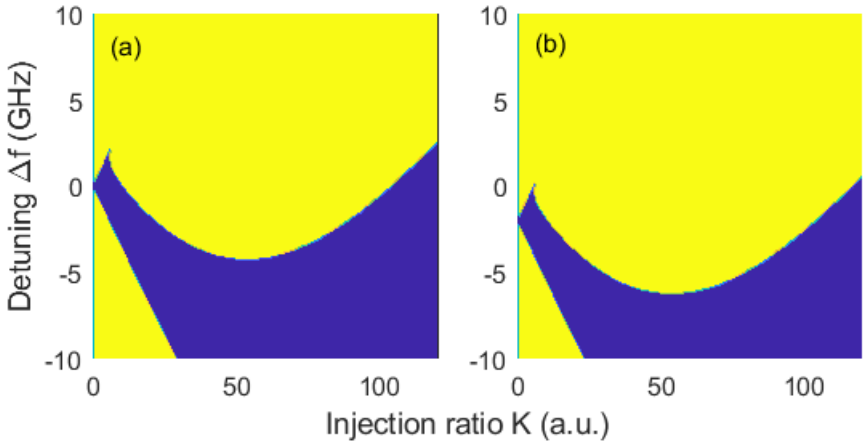


Figure 6. Stability diagram of two LCSLs under simultaneous external injection in the ( $K$ , $\Delta f$ ) plane, where $P = 2P_{th}$ , $d/a = 8$ , and $\Delta\Omega/2\pi = -2$ GHz . (a) laser A, and (b) laser B. Here, the purely real index guiding is considered.

One would be interested to see what happens for a very larger value of $d/a$ in the simultaneous external-injection scheme. To this end, we increase $d/a$ to 8 but keep other parameters same as those in Fig. 5(a). The resulting stability diagrams are shown in Fig. 6, (a) for laser A and (b) for laser B. We understand that when $d/a$ is very large, the coupling between lasers A and B is negligible, which means that they become isolated. In this case, the whole optically injected laser array can be seen as two isolated lasers subject to external injection from the same master laser. As expected, their stability maps are similar to that for a single optically injected laser[22]. We have assumed the frequency of laser A is equal to the reference frequency of the whole system, so that the left-most point of its stability region is located at zero value of the detuning frequency. For laser B, however, the whole stability domain is shifted down by the offset.

The results presented above for simultaneous external-injection are limited to the case of purely real index guiding. In fact, these also hold for the other waveguiding parameters listed in Table 1. Typical examples for positive index guiding with gain-guiding (second row in Table 1), pure gain guiding (third row in Table 1) and index antiguiding with gain-guiding (last row in Table 1) is shown in Fig. 7, where $P = 1.1P_{th}$ , $d/a = 2$ , and $\Delta\Omega/2\pi = -2$ GHz or $-6$ GHz. When comparing with Fig. 4, we observe that all the findings summarized above for the purely real index guiding can apply directly to the other three waveguide structures.

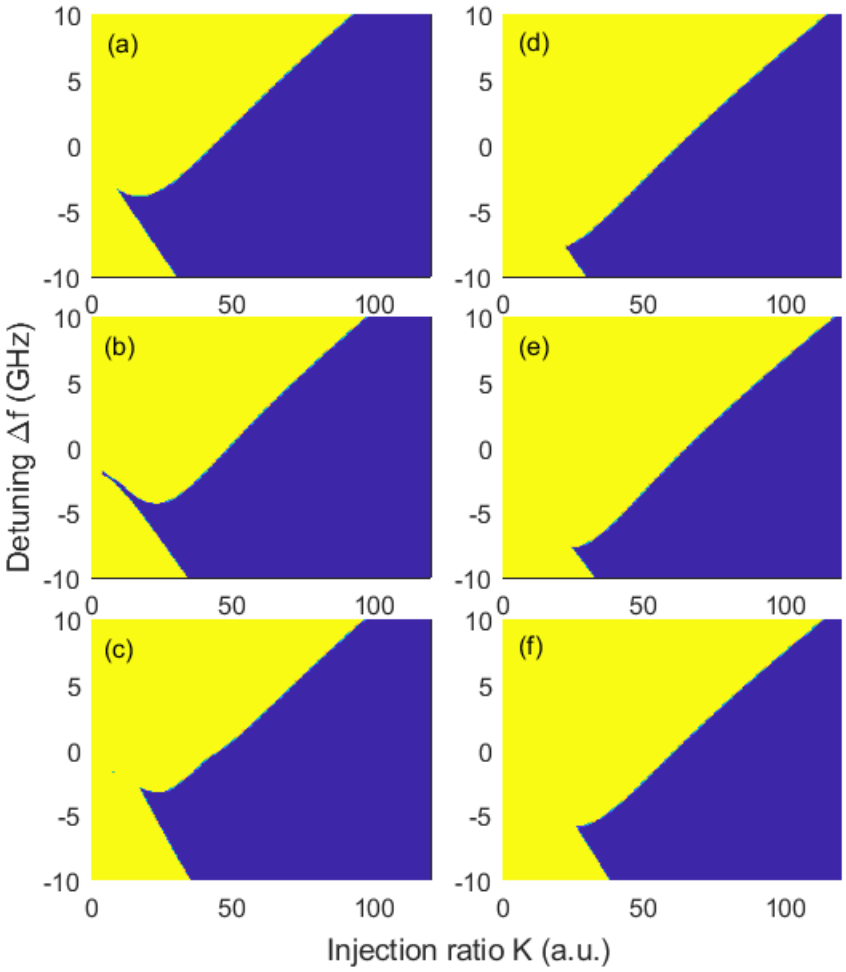


Figure 7. Stability diagram of two LCSLs under simultaneous external injection in the ( $K$ , $\Delta f$ ) plane, where $P = 1.1P_{th}$ , and $d/a = 2$ . First row: positive index guiding with gain-guiding, second row: pure gain guiding, and third row: index antiguiding with gain-guiding. Left column: $\Delta\Omega/2\pi = -2$ GHz , and right column: $\Delta\Omega/2\pi = -6$ GHz . Here, only the results for laser A are shown.

## 4. CONCLUSION

We have investigated the injection locking properties of two LCSLs subject to external injection for two different schemes: single or simultaneous external injection. In both schemes, we have constructed the stability diagrams which distinguish locked and unstable regions. We have considered and explained the influence of the waveguiding structures, the laser separation, the pump rate, and the frequency offset between the two coupled lasers. Our results compare the differences between these injection schemes. More importantly, these findings are not restricted by the waveguiding structures, so our results have a more general relevance to a better understanding of laser arrays subject to external optical injection.

## ACKNOWLEDGMENT

This work was supported by Engineering and Physical Sciences Research Council (Grant No. EP/M024237/1).

## REFERENCES

[1] Edited by Botez, D. and Scifres, D. R., Diode Laser Arrays, Cambridge University Press, Cambridge, 1994.
[2] Carlsson, N. W., Monolithic Diode-Laser Arrays, Springer-Verlag, Berlin, 1994.
[3] Blackbeard, N., Erzgräer, H. and Wieczorek, S., "Shear-induced bifurcations and chaos in models of three coupled lasers," SIAM J. Appl. Dyn. Syst. 10, 469 – 509 (2011).
[4] Blackbeard, N., Wieczorek, S., Erzgräer, H. and Dutta, P. S., "From synchronization to persistent optical turbulence in laser arrays," Physica D 286–287, 43 – 58 (2014).
[5] Winful, H. G., "Instability threshold for an array of coupled semiconductor lasers," Phys. Rev. A 46(9), 6093-6094(1992).
[6] Winful, H. G. and Rahman, L., "Synchronized chaos and spatiotemporal chaos in arrays of coupled lasers," Phys. Rev. Lett. 65(13), 1575 (1990).
[7] Ru, P., Jakobsen, P. K., Moloney, J. V. and India, R. A., "Generalized coupled-mode model for the multistripe index-guided laser arrays," J. Opt. Soc. Am. B 10, 507-515 (1993).
[8] Hess, O. and Schöll, E., "Spatio-temporal dynamics in twin-stripe semiconductor lasers," Physica D 70, 165-177(1994).
[9] Pimenov, A., Tronciu, V. Z., Bandelow, U. and Vladimirov, A. G., "Dynamical regimes of a multistripe laser array with external off-axis feedback," J. Opt. Soc. Am. B 30, 1606-1613 (2013).
[10] Auerbach, D. and Yorke, J. A., "Controlling chaotic fluctuations in semiconductor laser arrays," J. Opt. Soc. Am. B 13, 2178-2187 (1996).
[11] Münkel, M., Kaiser, F. and Hess, O., "Spatio-temporal dynamics of multi-stripe semiconductor lasers with delayed optical feedback," Phys. Lett. A 222, 67-75 (1996).
[12] Wilson, G. A., DeFreez, R. K. and Winful, H. G., "Modulation of phased-array semiconductor lasers at K-Band Frequencies," IEEE J. Quantum Electron. 27(6), 1696-1704 (1991).
[13] Erzgräber, H., Wieczorek, S. and Krauskopf, B., "Dynamics of two laterally coupled semiconductor lasers: Strong- and weak-coupling theory," Phys. Rev. E 78, 066201 (2008).
[14] Lamela, H., Leones, M., Carpintero, G., Simmendinger, C. and Hess, O. "Analysis of the dynamics behavior and short-pulse modulation scheme for laterally coupled diode lasers," IEEE J. Sel. Top. Quantum Electron. 7, 192-200 (2001).
[15] Wang, S. S. and Winful, H. G, "Dynamics of phase-locked semiconductor laser arrays," Appl. Phys. Lett. 52, 1774-1776 (1988).
[16] Winful, H. G. and Wang, S. S., "Stability of phase-locking in coupled semiconductor laser arrays," Appl. Phys. Lett. 53, 1894-1896 (1988).
[17] Lamela, H., Roycroft, B., Acedo, P., Santos, R. and Carpintero, G., "Experimental modulation bandwidth beyond the relaxation oscillation frequency in a monolithic twin-ridge laterally coupled diode laser based on lateral mode locking." Opt. Lett. 27, 303-305(2002).
[18] Santos, R. and Lamela, H., "Experimental observation of chaotic dynamics in two coupled diode lasers through lateral model locking," IEEE J. Quantum Electron. 45, 1490-1494 (2009).
[19] Hurtado, A., Mee, J., Nami, M., Henning, I. D., Adams, M.J. and Lester, L.F., "Tunable microwave signal generator with an optically-injected 1310nm QD-DFB laser," Opt. Express 21, 10772-10778 (2013).
[20] Li, N. Q., Pan, W., Yan, L. S., Luo, B., Zou, X. and Xiang, S. Y., "Enhanced two-channel optical chaotic communication using isochronous synchronization," IEEE J. Sel. Top. Quantum Electron., 19(4), 0600109 (2013).
[21] Li. N. Q., Kim, B., Chizhevsky, V. N., Locquet, A., Bloch, M., Citrin, D. S. and Pan, W., "Two approaches for ultrafast random bit generation based on the chaotic dynamics of a semiconductor laser," Opt. Express 22(6), 6634-6646(2014).

[22] Mogensen, F., Olesen, H. and Jacobsen, G., "Locking conditions and stability properties for a semiconductor laser with external light injection," IEEE J. Quantum Electron. QE-21, 784-793 (1985).
[23] Liu, Y., Liu, H. K. and Braiman, Y., "Simultaneous injection locking of couples of high-power broad-area lasers driven by a common current source," Appl. Opt. 41, 5036-5039 (2002).
[24] Long, C. M., Mutter, L., Dwir, B., Mereuta, A., Caliman, A., Sirbu, A., Iakovlev, V. and Kapon, E., "Optical injection locking of transverse modes in 1.3-*u*m wavelength coupled-VCSEL arrays," Opt. Express 22, 21137-21144 (2014).
[25] Quirce, A., Perez, P., Popp, A., Valle, A., Pesquera, L., Hong, Y. H., Thienpont, H. and Panajotov, K., "Polarization switching and injection locking in vertical-cavity surface-emitting lasers subject to parallel optical injection," Opt. Lett. 41, 2664-2667 (2016).
[26] Lau, E. K., Zhao, X. X, Sung, H. K., Parekh, D., Chang-Hasnain, C. and Wu, M. C., "Strong optical injection-locked semiconductor lasers demonstrating > 100-GHz resonance frequencies and 80-GHz bandwidths," Opt. Express 16, 6609-6618 (2008).
[27] Mercier, J. and McCall, M., "Stability and dynamics of an injection-locked semiconductor laser array," Opt. Commun. 138(1-3), 200-210 (1997).
[28] Goldberg, L., Taylor, H. F., Weller, J. F. and Scifres, D. R., "Injection locking of coupled stripe diode laser arrays," Appl. Phys. Lett. 46, 236-238 (1985).
[29] Adams, M. J., Li, N., Cemlyn, B. R., Susanto, H. and Henning, I. D., "Effects of detuning, gain-guiding and index antiguiding on the dynamics of two laterally-coupled semiconductor lasers," Phys. Rev. A 95, 053869 (2017).
[30] Li, N. Q., Susanto, H., Cemlyn, B. R., Henning, I. D. and Adams, M. J., "Locking bandwidth of two laterally-coupled semiconductor lasers subject to optical injection," Sci. Rep. 8, 109 (2018).
[31] Doedel, E. J., Champneys, A. R., Fairgrieve, T., Kuznetsov, Y., Oldeman, B., Pfaffenroth, R., Sandastede, B., Wang X. and Zhang, C., AUTO-07p: Continuation and Bifurcation Software for Ordinary Differential Equations (Concordia University, Montreal, 2008).
[32] Li, N. Q., Susanto, H., Cemlyn, B. R., Henning, I. D. and Adams, M. J., "Stability and bifurcation analysis of spin-polarized vertical-cavity surface-emitting lasers," Phys. Rev. A 96, 013840 (2017).